Asociación Argentina
de Mecánica Computacional

Mecánica Computacional Vol XLII, pp. 443-452
A. Caggiano, G. Etse, P. Folino, M. Goldschmit, M. Pucheta, M. Storti (Eds.)
L. Battaglia, H. Castro, M. Coussirat, R. Paz, S. Sarraf, A. Scarabino (Issue eds.)
Buenos Aires, November 11-14, 2025

INFLUENCE OF TURBULENCE MODEL ON THE FORM FACTOR DETERMINATION OF FISHING VESSELS

INFLUENCIA DEL MODELO DE TURBULENCIA EN LA DETERMINACIÓN DEL FACTOR DE FORMA DE BUQUES PESQUEROS

S. Oyuela[1,2], H. R. Díaz-Ojeda[3], A. D. Otero[1,4] and R. Sosa[1,2]

[1]*Universidad de Buenos Aires (UBA), Facultad de Ingeniería, Paseo Colón 850, Buenos Aires, C1063, Argentina, soyuela@fi.uba.ar*

[2]*CONICET - Universidad de Buenos Aires, Laboratorio de Ingeniería Naval y Oceánica (LabHiNO), Instituto de Tecnologías y Ciencias de la Ingeniería "Hilario Fernández Long" (INTECIN), Paseo Colón 850, Buenos Aires, C1063, Argentina, rsosa@fi.uba.ar*

[3]*Universidad de Las Palmas de Gran Canaria, Campus de Tafira, Las Palmas de Gran Canaria, 35017, España, hectorruben.diaz@ulpgc.es*

[4]*CONICET, Centro de Simulación Computacional para Aplicaciones Tecnológicas, Godoy Cruz 2390, Buenos Aires, C1425FQD, Argentina, aotero@fi.uba.ar*

Abstract. Turbulence modeling remains one of the primary sources of uncertainty in CFD, particularly in naval hydrodynamics. To avoid the high computational cost of directly resolving turbulent fluctuations, it is common practice to apply averaging methods and focus on the behavior of the mean flow. This introduces a closure problem in the fluid dynamic equations, which is typically addressed using two-equation models based on turbulent viscosity. In this study, three widely used turbulence models—k-ε, k-ω, and k-ω SST—were employed to perform single-phase simulations, evaluating their influence on the determination of the form factor of ship hulls. Each model was applied to the same set of case studies to assess the sensitivity of the form factor to turbulence modeling and to analyze how this sensitivity varies with Reynolds number in low length-to-beam ratio fishing vessels.

This work is part of a broader study on scale effects in power prediction for fishing vessels.

Keywords: Turbulence, form factor, CFD, OpenFOAM, RANS models, viscous resistance.

ISSN: 2591-3522 DOI: 10.70567/mc.v42.ocsid8247

1 INTRODUCTION

The prediction of the power required for a vessel to sail at its design speed is a central problem in naval engineering. Early studies by Froude (1874) established that a ship's total resistance can be decomposed into components that can be estimated separately, combining frictional resistance with a residual term. This decomposition is currently applied using the form factor $(1 + k)$ recommended by the ITTC (International Towing Tank Committee), which corrects the frictional resistance to account for pressure and wave-making effects, typically determined through the Prohaska method (26th ITTC Resistance Committee (2011)).

However, this approach assumes independence with respect to the Froude (Fr) and Reynolds (Re) numbers, leading to significant discrepancies between model-scale and full-scale vessels. In this context, Computational Fluid Dynamics (CFD) emerges as a complementary tool to analyze three-dimensional viscous flows under controlled conditions. One of the main sources of uncertainty in CFD is turbulence modeling. To avoid the high computational cost of directly resolving turbulent fluctuations, averaging methods are applied to characterize the global flow behavior (Durbin and Reif, 2011; Ferziger and Springer, 2003; Wilcox, 2006), resulting in an unclosed system of equations that is commonly closed using two-equation turbulence models based on turbulent viscosity. These models additionally solve for the turbulent kinetic energy (k) and a measure of the decay of turbulent eddies, represented by either the turbulent dissipation rate (ε) or the specific dissipation rate (ω).

In this study, four widely used turbulence models were compared: $k-\omega$, $k-\omega$ SST, standard $k-\varepsilon$, and realizable $k-\varepsilon$, implemented in `OpenFOAM v11`. As discussed in Wilcox (2006); Menter (1994), the $k-\omega$ model provides good near-wall resolution but can be sensitive to boundary conditions; the $k-\omega$ **SST** model combines the near-wall robustness of $k-\omega$ with the performance of $k-\varepsilon$ in the outer regions, improving predictions in separated flows. The standard $k-\varepsilon$ model is robust and efficient, though less accurate in regions with high pressure gradients or flow separation, whereas the **realizable** variant ensures mathematical consistency and better represents flows with rotation, curvature, and moderate separation.

This work applies these CFD simulations to a fishing vessel at different scales, comparing friction, pressure, and form factor coefficients, and evaluating how the choice of turbulence model affects both model-scale and full-scale extrapolations.

2 METHODOLOGY

2.1 Form Factor

The form factor allows the calculation of viscous resistance from the frictional resistance of an equivalent flat plate. Experimentally, it is estimated using the Prohaska method 26th ITTC Resistance Committee (2011), extrapolating the resistance to very low speeds ($Fr \approx 0$), where wave-making resistance is negligible.

In CFD, only the submerged portion of the hull is simulated with a symmetry condition at the waterline, removing the air phase and free surface. Thus, the dimensionless total resistance C_V from the simulation consists of the tangential (frictional, C_F) and normal (pressure, C_{PV}) components, without any wave contribution (C_W). From the original expression of Hughes (1954):

$$C_T = (1 + k)C_{F0} + C_W,$$

one obtains:

$$C_V = (1+k)C_{F0} = C_F + C_{PV}, \quad 1+k = \frac{C_V}{C_{F0}} = \frac{C_F + C_{PV}}{C_{F0}},$$

where C_{F0} is obtained from the ITTC-57 correlation (26th ITTC Resistance Committee, 2011) for the same Re. All forces are nondimensionalized as:

$$C_X = \frac{F_X}{\frac{1}{2}\rho S V^2},$$

with F_X the corresponding force, ρ the water density, S the wetted surface area, and V the relative velocity between the hull and the water.

2.2 Experimental Facilities

The resistance tests were conducted in the towing tank of the Naval and Ocean Hydrodynamics Laboratory (LabHiNO) at the University of Buenos Aires (UBA), Argentina. The model was carefully ballasted to meet the target displacements and waterlines before being mounted on a Kempf & Remmers R 47 load cell. The connection to the carriage via this load cell constrained pitch, yaw, and roll motions, allowing the model to freely adjust its trim and sinkage. The load cell, designed for forces up to ±100 N, had a sensitivity of approximately ±1 mV/V of supply voltage.

Regarding the model's transverse midship section, it represented approximately 1.2

The experimental setup and uncertainty analysis for the model were previously described in Oyuela et al. (2024). Tests were carried out following ITTC guidelines (26th ITTC Resistance Committee, 2011), with estimated uncertainties in resistance measurements ranging from 0.83

2.3 Numerical Model

All simulations were carried out using the open-source finite volume code OpenFOAM 11. This study is based on the configurations adopted in Oyuela et al. (2024), where the numerical parameters are described in detail.

Turbulent flow was modeled using the Reynolds-Averaged Navier–Stokes (RANS) equations with the PIMPLE algorithm for pressure–velocity coupling, which is suitable for transient simulations with high Courant numbers. The *localEuler* scheme was used for time advancement. Convergence was assessed by monitoring force fluctuations, ensuring they remained below 1

The numerical domain, shown in Figure 1, follows ITTC recommendations (28th ITTC Resistance Comittee, 2017). The inlet was located 1.5 hull lengths upstream of the bow perpendicular, with a uniform velocity condition. The outlet was placed 2.5 hull lengths downstream of the stern perpendicular, with a zero-gradient condition for all variables. Lateral and bottom walls were positioned 2.5 hull lengths from the hull centerline, imposing symmetry conditions to minimize blockage effects. At the free surface, a symmetry condition was applied at the draft plane, considering that only single-phase, double-body-like simulations were performed. The hull was treated as a no-slip wall and regarding rugosity, based on ITTC guidelines (26th ITTC Resistance Committee, 2011), the hull surface was assumed to be hydraulically smooth in the CFD simulations for all scales.

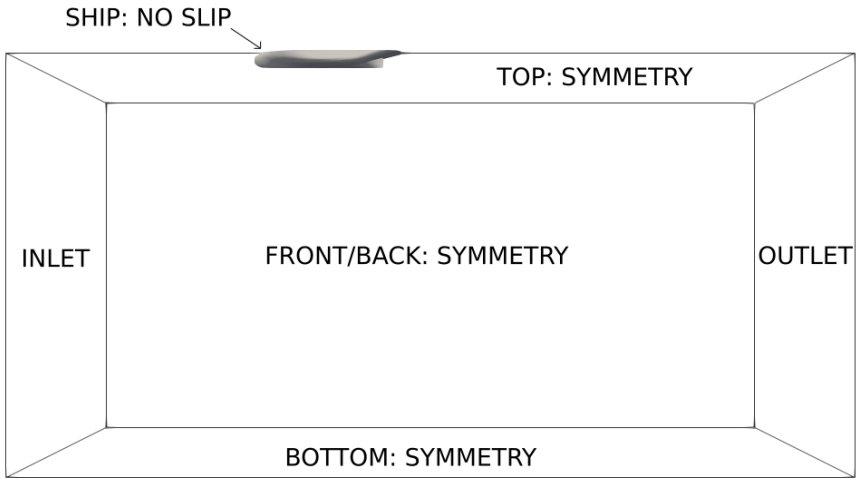

Figure 1: Computational domain.

3 GEOMETRY AND SCALES

A low length-to-beam ratio (L/B) fishing vessel was selected as the case study and analyzed at three geometric scales: $\lambda = 20$, $\lambda = 5$, and $\lambda = 1$ (full scale). The 1:20 scale model was constructed following ITTC recommendations (Specialist Committee: Procedures for Resistance and of 23rd ITTC 2002, 2002), ensuring structural integrity and surface smoothness. Figure 2 shows the 1:20 scale model in side view, perspective view, and lines plan.

The main dimensions of the full-scale vessel and the reduced-scale models are summarized in Table 1.

Parameter (Symbol)	**Unit**	**Full Scale** ($\lambda = 1$)	**Model (1:5)**	**Model (1:20)**
Scale (λ)	-	1	5	20
Waterline length (L_{WL})	m	32.680	6.536	1.641
Overall length (L_{OS})	m	34.795	6.959	1.670
Beam (B)	m	9.280	1.856	0.464
Draft (T)	m	3.300	0.660	0.195
Displacement (∇)	m^3	599.400	4.795	0.095
Wetted surface (S)	m^2	392.670	15.707	1.124
Block coefficient (C_B)	-	0.600	0.600	0.600
Midship coefficient (C_M)	-	0.860	0.860	0.890
Reynolds number (Re)	-	1×10^8	1×10^7	1×10^6

Table 1: Main dimensions of the fishing vessel at full scale and reduced-scale models.

With these dimensions, the Reynolds and Froude numbers are defined as:

$$Re = \frac{V L_{OS}}{\nu}, \quad Fr = \frac{V}{\sqrt{g L_{WL}}},$$

where V is the vessel speed, ν the kinematic viscosity, and g the gravitational acceleration.

(a) Side view.

(b) Perspective view.

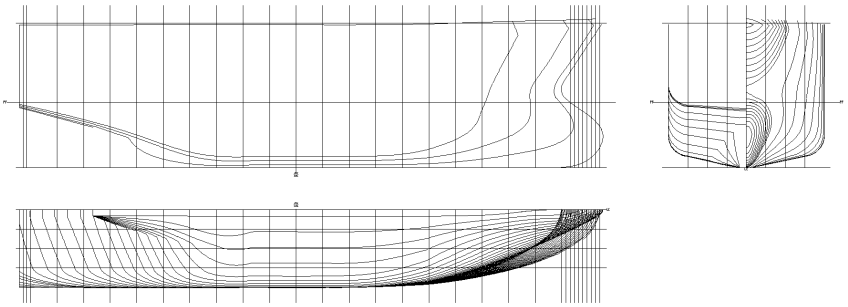

(c) Lines plan.

Figure 2: 1:20 scale model of the fishing vessel: (a) side view, (b) perspective view, (c) lines plan.

4 RESULTS

Figure 3 presents the dimensionless viscous resistance C_V, and Figure 4 compares the resulting form factor obtained by simulating with the different turbulence models analyzed, together with the experimental value obtained via the Prohaska method for the 1:20 scale. The latter, according to the currently recommended extrapolation method, is assumed constant for all studied scales. In Oyuela et al. (2024), it was shown that simulating a double-body configuration with the $k-\omega$ SST model returned values at low Fr similar to the experimental method. A subsequent study showed that the slope of the form factor with increasing Re is linked to the L/B ratio, with low L/B ratios responsible for its increase. In this work, it is interesting to observe the behavior of the other turbulence models under the same condition.

At low Re, where the numerical results can be validated against experimental data, the other three turbulence models tested show significant differences compared to $k-\omega$ SST. Not surprisingly, the least accurate is $k-\varepsilon$, due to its inability to handle near-wall flows. The realizable $k-\varepsilon$ model improves this prediction but still remains far from the experimental value, followed by $k-\omega$. It should be noted that none of these models were designed to precisely model the laminar-to-turbulent transition. In Karim et al. (2011), the experimental resistance of a fully submerged body with $L/B=4$ at $Re=2\times10^7$ was compared against the turbulence models used in this work, resulting in an overestimation by $k-\omega$, followed by $k-\varepsilon$, then realizable $k-\varepsilon$, with the closest match to the experimental value given by $k-\omega$ SST. This agrees with the results at the same Re shown in Figure 3.

As shown in Figure 4, as Re increases, the form factor curves of $k-\omega$ SST and realizable $k-\varepsilon$ asymptotically approach each other, while $k-\varepsilon$, although still showing some difference, reproduces the same trend. In the case of $k-\omega$, the form factor increases significantly around

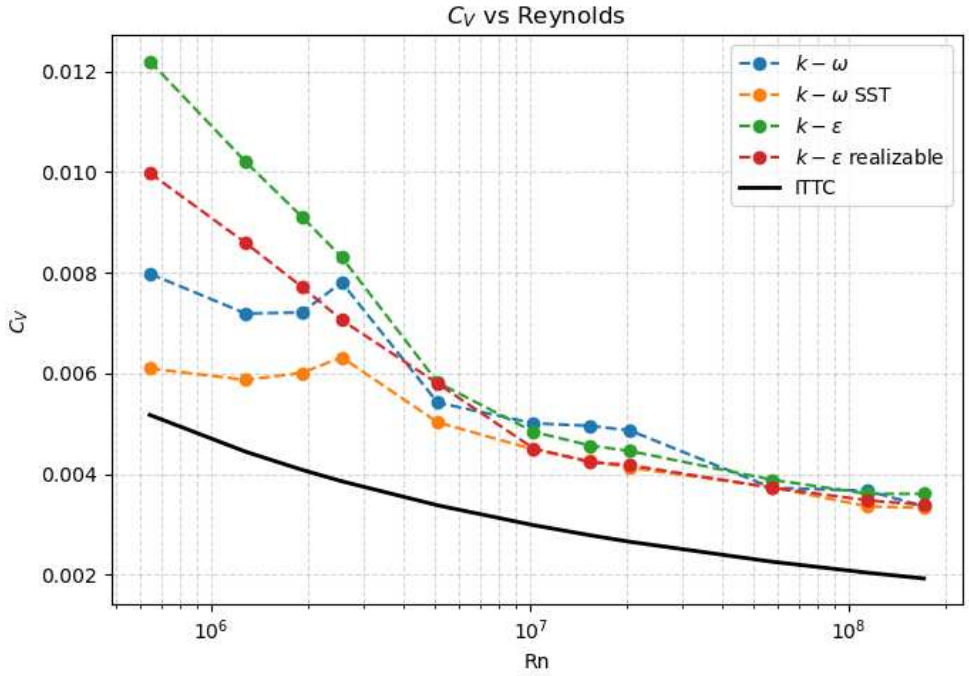

Figure 3: Dimensionless viscous resistance C_V as a function of Re, obtained using different turbulence models.

$Re = 2 \times 10^7$ due to the previously discussed rise in resistance, then decreases approaching the $k - \varepsilon$ trend.

The frictional force, shown in Figure 5, indicates that $k-\omega$ SST closely follows the ITTC-57 correlation line throughout most of the range, except at the lowest Re values, where the flow is primarily in a transitional regime. From $Re = 1 \times 10^7$ onwards, friction is modeled similarly in all cases except for $k - \omega$.

For the viscous pressure force presented in Figure 6, smaller differences between the models are observed. This is further quantified in Figure 7, where these differences are evaluated.

5 DISCUSSION

In contrast to the results reported by Terziev et al. (2021) for the KCS (Kriso Container Ship), in our study of the fishing vessel we do not observe the same behavior among the evaluated turbulence models. In their case, the form factor obtained with $k - \omega$ SST always lies between the values obtained using $k - \omega$ and $k - \varepsilon$, which is justified by the fact that $k - \omega$ SST is a combination of the other two models. In our case, however, $k-\omega$ SST yields the lowest values.

This difference can be explained by relevant geometric variations: the container ship studied in (Terziev et al., 2021) has a high length-to-beam ratio ($L/B > 7$) and smoother lines, whereas the fishing vessel has $L/B < 4$ and sharper geometric transitions. These differences result in less pronounced pressure gradients and a lower tendency for strong flow separation in the KCS, conditions under which the four turbulence models behave more similarly. In the fishing vessel, higher curvature and local gradients increase the sensitivity of each model to separation and recirculation phenomena.

Figure 7 shows stacked bars as a function of Reynolds number, illustrating, for the fishing vessel, the differences in C_F and C_{PV} between the turbulence models k-ε, k-ω, and realizable k-ε relative to k-ω **SST**. This allows observing how the relative contribution of each component

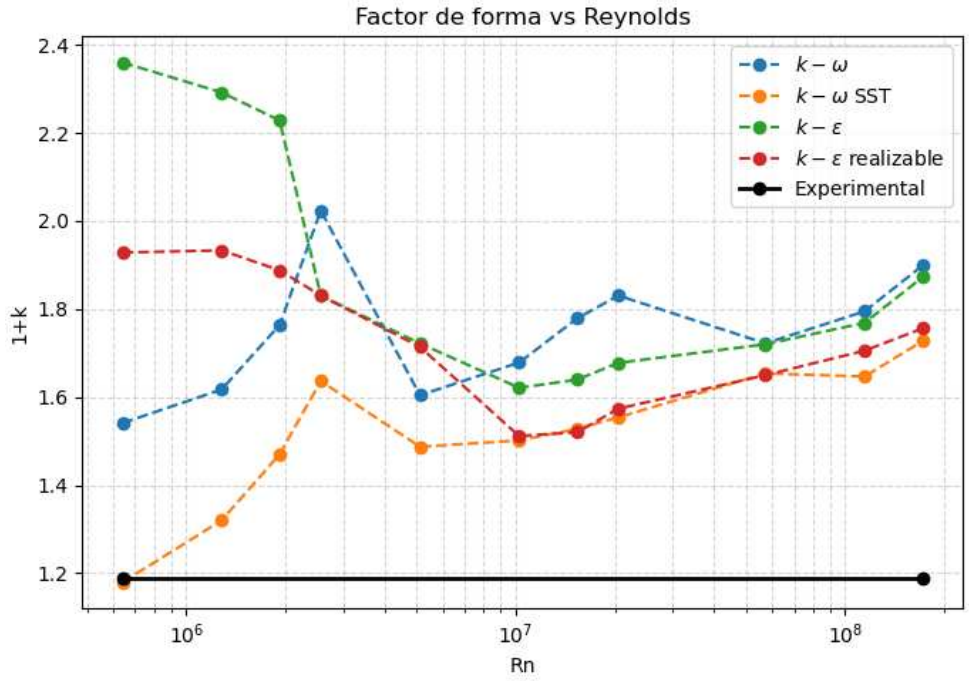

Figure 4: Form factor $1 + k$ as a function of Re, obtained using different turbulence models.

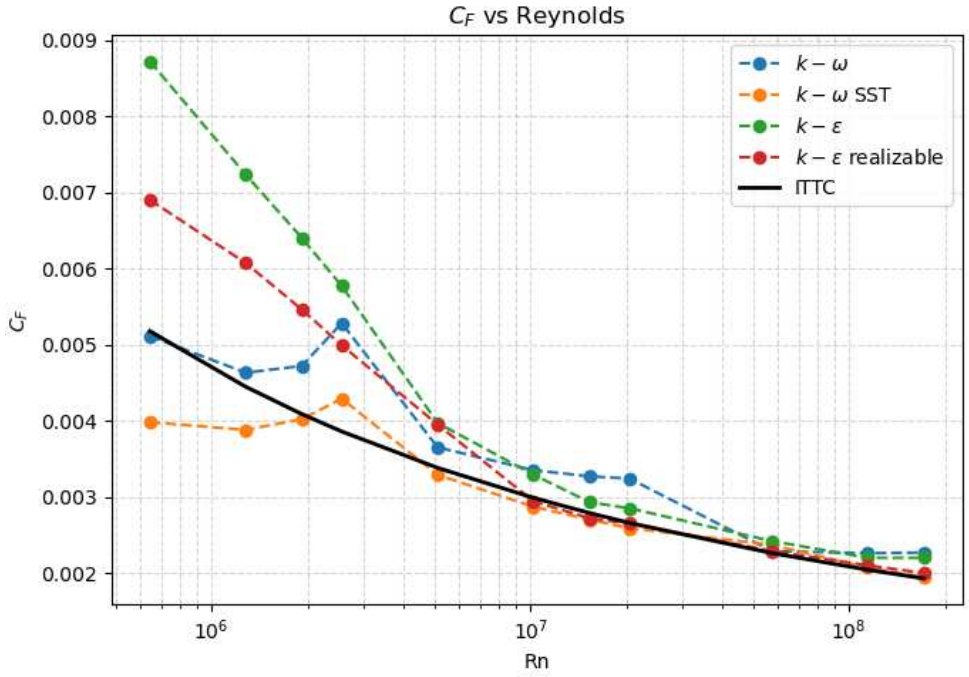

Figure 5: Friction coefficient C_F as a function of Re, obtained using different turbulence models.

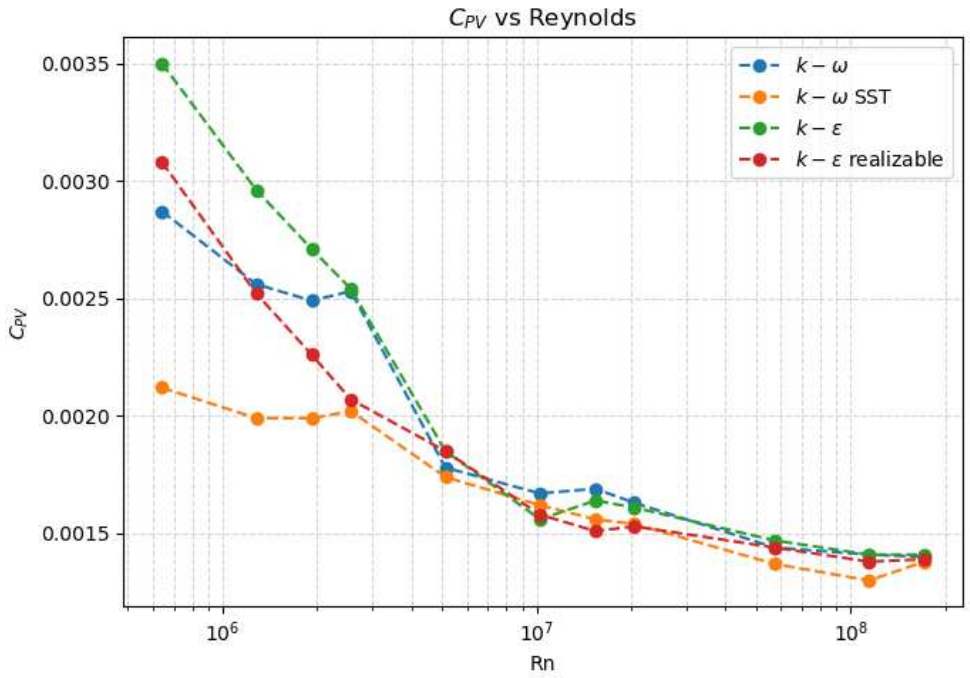

Figure 6: Viscous pressure coefficient C_{PV} as a function of Re, obtained using different turbulence models.

varies depending on the model used and the Re regime considered. A larger spread in C_F among models is seen at low Re, resulting in a larger difference in total resistance due to the dominant contribution of friction in this regime. As C_F asymptotically approaches the ITTC correlation line for all models and its relative weight decreases, the differences between models diminish. For C_{PV}, a convergence among models is also observed, and, except for some cases, its relative contribution to the total resistance generally increases. This relative increase in C_{PV} is responsible for the observed rise in the form factor.

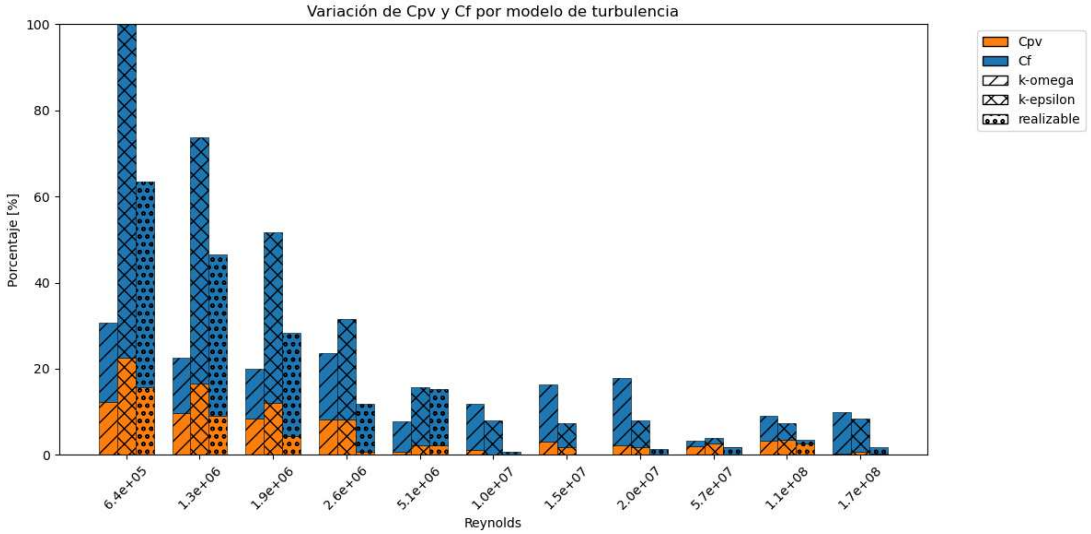

Figure 7: Difference in percentage points relative to k-ω SST for the frictional and viscous pressure components of total resistance.

6 CONCLUSIONS

At low Reynolds numbers, the choice of turbulence model has a significant impact on the estimation of the form factor. Among the models analyzed, $k-\omega$ SST most accurately reproduces the experimental Prohaska values, whereas the standard $k-\varepsilon$ and realizable $k-\varepsilon$ show considerable deviations, mainly due to their reduced capability to model near-wall flows and the laminar-to-turbulent transition. As Re increases, the differences between models decrease, particularly for C_F, where all models converge toward the ITTC correlation, showing similar values of $1+k$. This indicates that the selection of the turbulence closure is critical at reduced scales but less relevant at full scale.

The analysis also shows that at low Re, friction contributes most to the differences in the calculated form factor. Careful validation of turbulence models is essential for reliably extrapolating numerical results to full-scale conditions.

7 ACKNOWLEDGMENTS

This work was funded by the Ministry of Science, Technology and Innovation of the Argentine Republic (MINCyT; Research and Technological Development Project of the Pampa Azul Initiative – B2), the University of Buenos Aires, Faculty of Engineering (Peruilh Fellowship), and the Ministry of Science and Innovation of Spain through the grant PID2022-140481OB-I00.

Computational resources were provided by the Tupac cluster (https://www.tupac.gob.ar) and the UNC Supercomputing Center (CCAD) at the National University of Córdoba (https://supercomputo.unc.edu.ar), which are part of the National High-Performance Computing System (SNCAD) of the Argentine Republic.

REFERENCES

26th ITTC Resistance Committee. *ITTC – Recommended Procedures and Guidelines - Resistance Test*. ITTC, 2011.

28th ITTC Resistance Comittee. *ITTC, 2017. Uncertainty analysis in cfd verification and validation, methodology and procedures. ITTC - Quality System Manual Recommended Procedures and Guidelines 7, 5-03-01-01.* ITTC, 2017.

Durbin P.A. and Reif B.P. *Statistical theory and modeling for turbulent flows*. John Wiley & Sons, 2011.

Ferziger J.H. and Springer M.P. Computational methods for fluid dynamics: Third edition. *Computers & Mathematics with Applications*, 46(2):503–504, 2003. ISSN 0898-1221. http://doi.org/https://doi.org/10.1016/S0898-1221(03)90046-0.

Froude W. On experiments with h.m.s. greyhound. *Transactions of the Royal Institution of Naval Architects*, 15:36–73, 1874.

Hughes G. Friction and form resistance in turbulent flow, and a proposed formulation for use in model and ship correlation. *National Physical Laboratory, NPL, Ship Division, Presented at the Institution of Naval Architects, Paper No. 7, London, April, RINA Transactions 1954-16*, 1954.

Karim M., Rahman M., and Alim M.A. Performance of sst k-ω turbulence model for computation of viscous drag of axisymmetric underwater bodies. *International Journal of Engineering*, 24, 2011.

Menter F.R. Two-equation eddy-viscosity turbulence models for engineering applications. *AIAA Journal*, 32(8):1598–1605, 1994. http://doi.org/10.2514/3.12149.

Oyuela S., Ojeda H.R.D., Arribas F.P., Otero A.D., and Sosa R. Investigating fishing ves-

sel hydrodynamics by using efd and cfd tools, with focus on total ship resistance and its components. *Journal of Marine Science and Engineering*, 12(4), 2024. ISSN 2077-1312. http://doi.org/10.3390/jmse12040622.

Specialist Committee: Procedures for Resistance P. and of 23rd ITTC 2002 P.O.W.T. *ITTC – Recommended Procedures and Guidelines: Model Manufacture, Ship Models*. ITTC, 2002.

Terziev M., Tezdogan T., Demirel Y.K., Villa D., Mizzi S., and Incecik A. Exploring the effects of speed and scale on a ship's form factor using cfd. *International Journal of Naval Architecture and Ocean Engineering*, 13:147–162, 2021. ISSN 2092-6782. http://doi.org/https://doi.org/10.1016/j.ijnaoe.2020.12.002.

Wilcox D.C. *Turbulence Modeling for CFD*. DCW Industries, Inc., La Cañada, California, 3 edition, 2006.